

RESEARCH ARTICLE

Descending Vasa Recta Endothelial Membrane Potential Response Requires Pericyte Communication

Zhong Zhang, Kristie Payne, Thomas L. Pallone*

Division of Nephrology, Department of Medicine, University of Maryland School of Medicine, Baltimore, Maryland 21201, United States of America

* tpallone@medicine.umaryland.edu



Abstract

Using dual-cell electrophysiological recording, we examined the routes for equilibration of membrane potential between the pericytes and endothelia that comprise the descending vasa recta (DVR) wall. We measured equilibration between pericytes in intact vessels, between pericytes and endothelium in intact vessels and between pericytes physically separated from the endothelium. Dual pericyte recording on the abluminal surface of DVR showed that both resting potential and subsequent time-dependent voltage fluctuations after vasoconstrictor stimulation remained closely equilibrated, regardless of the agonist employed (angiotensin II, vasopressin or endothelin 1). When pericytes were removed from the vessel wall but retained physical contact with one another, membrane potential responses were also highly coordinated. In contrast, responses of pericytes varied independently when they were isolated from both the endothelium and from contact with one another. When pericytes and endothelium were in contact, their resting potentials were similar and their temporal responses to stimulation were highly coordinated. After completely isolating pericytes from the endothelium, their mean resting potentials became discordant. Finally, complete endothelial isolation eliminated all membrane potential responses to angiotensin II. We conclude that cell-to-cell transmission through the endothelium is not needed for pericytes to equilibrate their membrane potentials. AngII dependent responses of DVR endothelia may originate from gap junction coupling to pericytes rather than via receptor dependent signaling in the endothelium, per se.

OPEN ACCESS

Citation: Zhang Z, Payne K, Pallone TL (2016) Descending Vasa Recta Endothelial Membrane Potential Response Requires Pericyte Communication. PLoS ONE 11(5): e0154948. doi:10.1371/journal.pone.0154948

Editor: Mauricio Sendeski, Charité Universitätsmedizin Berlin, GERMANY

Received: January 13, 2016

Accepted: April 21, 2016

Published: May 12, 2016

Copyright: © 2016 Zhang et al. This is an open access article distributed under the terms of the [Creative Commons Attribution License](https://creativecommons.org/licenses/by/4.0/), which permits unrestricted use, distribution, and reproduction in any medium, provided the original author and source are credited.

Data Availability Statement: All relevant data are within the paper and its Supporting Information files.

Funding: This work was supported by the National Institutes of Health, NIDDK, R01DK042495, R01DK067621.

Competing Interests: The authors have declared that no competing interests exist.

Introduction

Descending vasa recta (DVR) are arteriolar microvessels that supply blood flow to the renal medulla. Their wall is comprised of a continuous endothelium surrounded by smooth muscle-like pericytes [1–3] whose contractile activity involves activation of voltage gated calcium entry pathways [4, 5]. In turn, the membrane potential that governs voltage gated calcium channel (VGCC) activity is largely governed by the balanced activities of K⁺ and Cl⁻ channel conductance. Application of a vasoconstrictor, such as angiotensin II (AngII) activates calcium

dependent chloride channels (CaCC) and leads to delayed suppression of K^+ channels leading to depolarization [6, 7]. An important feature of the DVR wall, and microvessels of other organs in general, is that mural cells (smooth muscle, endothelia) can modify one another's membrane potential by electrical conduction across gap junctions [8, 9]. It is generally believed that such intercellular communication in small microvessels can extend the range of stimuli at one location so to reach distant points along the vessel axis. In the renal medulla, for example, this favors the hypothesis that mediators released in response to outer medullary hypoxia might transmit their actions through the DVR syncytium to dilate upstream, parent juxtamedullary efferent arterioles.

Experimental modification of syncytial communication between smooth muscle (e.g., pericytes) and endothelium is difficult because chemical gap junction blockade can have nonspecific effects on channel activity and other membrane proteins [10]. Similarly, genetic disruption of constituent connexin subunits that comprise gap junctions may alter expression of other connexin isoforms or modify the heterologous combinations that form assembled connexon proteins [9]. In this effort we used an alternative approach, physical disruption of contact between cells, to test for presence of communicative pathways. We removed abluminal pericytes and performing dual-cell homologous or heterologous recording from pericytes and endothelia to assess the persistence of membrane potential equilibration, both at rest and during response to contractile agonists. In some experiments, pericytes were fully separated from the endothelium to test whether such disruption modifies or eliminates responses of either cell type to AngII. We found that all pericytes on an isolated DVR segment maintain equal resting potentials and that such coupling persists during depolarization from AngII, arginine vasopressin (AVP), or endothelin 1 (ET1). No constrictor modified capacity for pericyte-to-pericyte coordination. Pericytes fully separated from one another depolarized but could not coordinate their responses. Finally, after complete pericyte removal, depolarizing responses in the isolated endothelium was eliminated. These results show that pericyte-to-endothelial electrical conduction is not needed to coordinate pericyte response; however pericyte contact is needed to achieve endothelial response.

Materials and Methods

Isolation of DVR

This study was carried out in strict accordance with the recommendations in the Guide for the Care and Use of Laboratory Animals of the National Institutes of Health. The protocol was approved by the Committee on the Ethics of Animal Experiments of the University of Maryland (IACUC Protocol number: 1113009). All surgery was performed under ketamine / xylazine anesthesia, and all efforts were made to minimize suffering. Sprague Dawley rats (120–200 g; Harlan) were anesthetized by an intraperitoneal injection of ketamine / xylazine (80 mg/kg / 10 mg/kg), following which kidneys were harvested and sectioned as previously described [7, 11]. Tissue slices were stored at 4°C in physiological saline solution (PSS, in mM) NaCl 145, KCl 5, $MgCl_2$ 1, $CaCl_2$ 1, N-2-hydroxyethylpiperazine-N'-2-ethanesulfonic acid (HEPES) 10, osmolality ~356 mOsm/Kg H_2O , glucose 10, pH 7.4 at room temperature). To permit formation of gigaseals during patch clamp, tissue wedges comprised of cortex, outer and inner medulla were digested at 37°C for ~22 minutes in a collagenase 1A (0.5 mg/ml), protease XIV (0.4 mg/ml) and bovine serum albumin (1.0 mg/ml) in calcium free PSS. After digestion, the tissue was stored in calcium replete PSS at ~4°C. DVR segments were isolated from inner stripe vascular bundles by hand dissection and transferred to a chamber on an inverted microscope for patch clamp [7]. Access to endothelia was achieved by complete or partial pericyte removal from the abluminal surface. As previously described and illustrated, pericytes were sheared

off the wall of collagenase treated vessels when they were drawn into, and then ejected from, a micropipette whose orifice had been heat polished to ~6 microns [12].

Whole cell patch clamp recording

Patch clamp electrodes were constructed from borosilicate capillary tubes (PG52151-4, external diameter 1.5 mm, internal diameter 1.0 mm; World Precision Instruments, Sarasota, FL), with a two-stage vertical pipette puller (Narshige PP-830) followed by heat polishing of their tips. Whole-cell electrical access was achieved using nystatin (100 microg/ml) as the pore forming agent [6, 7]. The electrode buffer was (in mmol/L): KAspartate 120, KCl 20, NaCl 10, HEPES 10, osmolality ~320 mOsm/Kg H₂O, pH 7.2. The extracellular buffer was PSS. The bath was introduced by gravity into a custom constructed chamber and drawn away by suction. The geometry of the chamber has been previously described [7]. Briefly, it has a narrow channel where the bath electrode Ag/AgCl wire is placed. The preparation is immobilized just downstream of the wire and buffer entry point. Downstream of the narrow channel the chamber enlarges to a wide portion where flowing bath is removed by suction. This configuration provides for rapid exchange of reagents in the vicinity of the preparation with minimization of electrical noise. Dual cell recordings were performed at room temperature with a Multiclamp 700B amplifier as previously described [13]. Quality of gigaseals was verified using Clampex 10 and membrane potential was recorded with zero current clamp protocols [7]. In some voltage clamp experiments we imposed square wave membrane potential deviations on a pericyte from a holding level of -80 mV to -40 mV while recording membrane potential of distant endothelial cells by zero current clamp at 10 Hz. Those protocols were executed with Clampex and the recordings digitized using a Digidata 16 bit analog-to-digital converter (Molecular Devices). Results were corrected for junction potentials [7].

Reagents

Nystatin, angiotensin II, vasopressin, endothelin, heptanol 18BGR, collagenase 1A, protease XIV and other chemicals were from Sigma (St Louis, MO). Reagents were thawed and diluted on the day of the experiment and excess discarded daily.

Statistics

Data in the text and figures are reported as mean \pm SE. For all protocols, one DVR was analyzed per rat for inclusion in the summarized results. Experiments in which gigaseals failed before or during data acquisition were discarded. Correlations were analyzed by linear regression. Sequential measurements in individual DVR were analyzed by repeated measures ANOVA using Holm-Sidak post hoc multiple comparison testing with SigmaStat 3.11 (Systat Software, Inc., Point Richmond, CA).

Results

Dual pericyte membrane potential recording, intact DVR

In a first series, we tested the extent to which pericytes of a single DVR share membrane potential, both at rest and during agonist induced depolarizations. Three agents known to constrict DVR were studied, AngII (10 nM), AVP (100 nM) and ET1 (1 nM). We chose the respective concentrations to match those that generated maximal vasoconstriction of microperfused DVR in past studies [14–16]. Dual pericyte recordings were performed in DVR from 5 rats per constrictor (1 DVR per rat, N = 15 rats total). No vessel was exposed to more than one agent. The correlation between resting membrane potentials is shown in Fig 1 where the dashed line is the best-fit linear regression (F = 31.8, DF = 14, R = 0.84, P < 0.001). Close approximation of

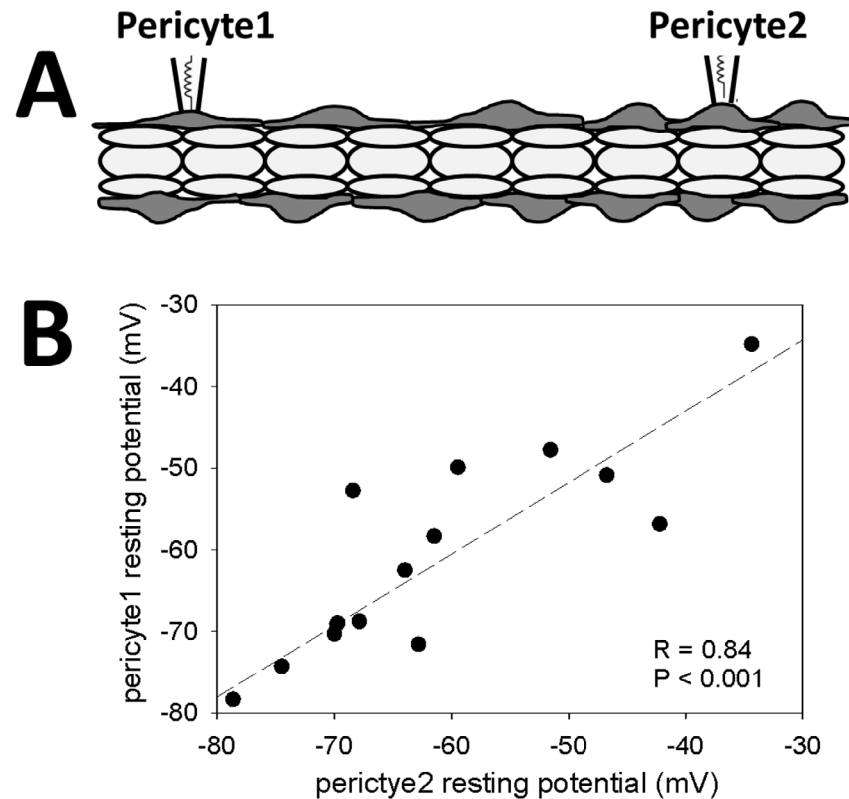


Fig 1. Dual pericyte patch clamp configuration and resting potentials. **A.** Dual recordings of membrane potential were performed on pericytes (dark gray) of intact DVR with endothelium (light gray) present. **B.** Each data point shows the initial resting potentials recorded from two pericytes of the same DVR (N = 15). The dashed line shows the best fit linear regression (R = 0.84, P < 0.001).

doi:10.1371/journal.pone.0154948.g001

resting potential of pericytes along the intact DVR wall was consistently observed (pericyte1 vs pericyte2, mean \pm SEM: -61 ± 2.7 mV vs -61 ± 2.6 mV, N = 15).

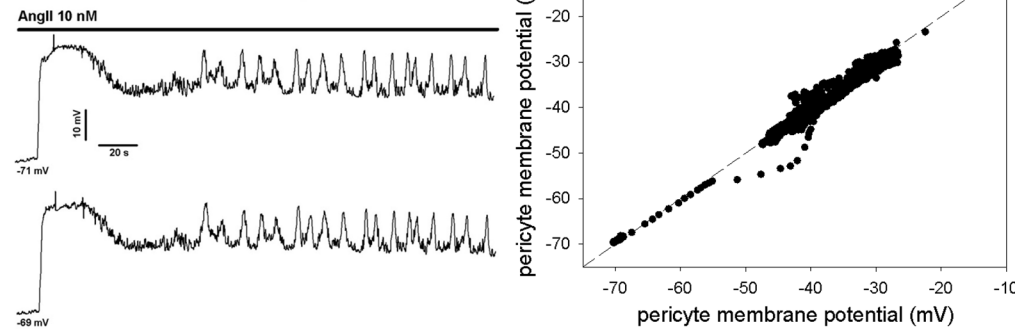
Examples of time-dependent changes in pericyte membrane potential during exposure to vasoconstrictors are shown in Fig 2. Regardless of the agent used, AngII (Fig 2A), AVP (Fig 2B), or ET1 (Fig 2C), depolarization of two pericytes always occurred together in a similar pattern with membrane potentials retaining near-identity. Syncytial coordination was maintained and no agent interfered with gap junction coupling. We calculated the difference between pericyte membrane potentials at each time point during the responses and averaged the results to quantify the degree of equilibration. Those time-averaged differences were 0.29 ± 0.34 mV, 1.5 ± 1.20 mV, and 0.29 ± 0.34 mV (mean \pm SEM) for AngII, AVP and ET1, respectively. The differences were not significantly different from zero (within two standard errors). There were no significant differences between time averaged pericyte membrane potentials for any vasoconstrictor (paired t-test) nor was there a difference between the magnitude of depolarization achieved by AngII, AVP or ET1 (ANOVA). Summaries of the equilibrations are provided in Table 1 where the correlation coefficients (R values), number of data points recorded and P values for the linear regressions have been summarized as mean \pm SEM.

Dual recordings from pericytes in isolation

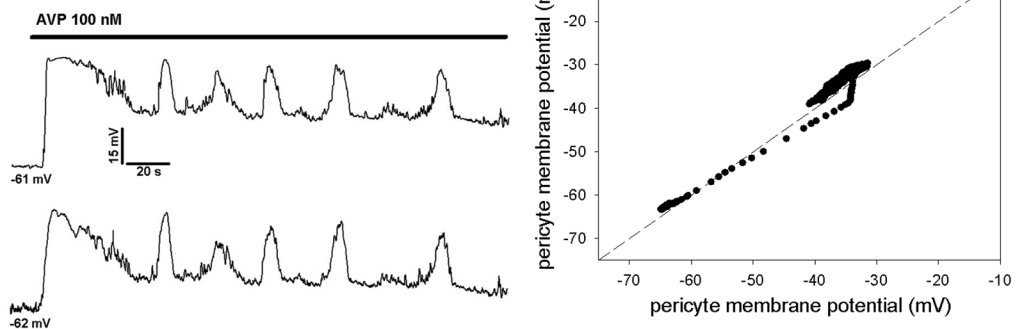
The close similarity of membrane potentials between pericytes (Figs 1 and 2) might be accounted for by conduction between pericytes, per se, or by conduction from pericyte to

endothelium and back to nearby pericytes. To determine whether pericyte-to-pericyte conduction could account for the coordination, we removed pericytes from the DVR wall and placed them on coverslips. Two configurations were used, one in which accessed pericytes retained physical contact with one another (Fig 3A and 3B, abbreviated P-P), and another where spatial

A - AngII



B - AVP



C - ET1

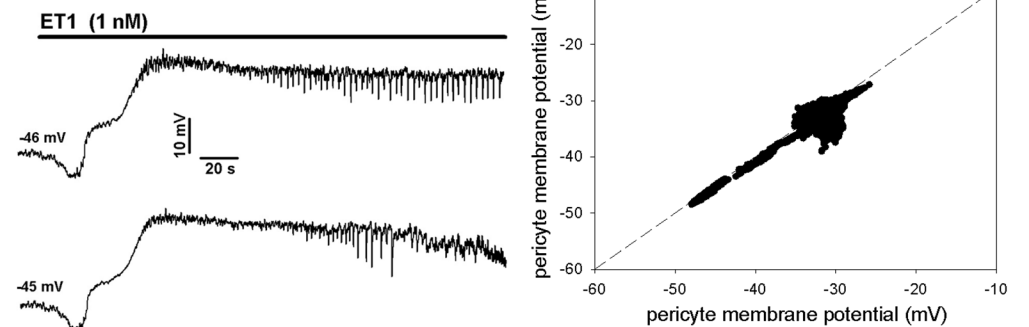


Fig 2. Simultaneous membrane potential recording in two pericytes during exposure to vasoconstrictors.
A. AngII: Left panel shows an example of membrane potential responses of two pericytes on a DVR during exposure to AngII (10 nM, similar to $n = 5$). Resting potentials prior to AngII were -71 mV and -69 mV. **B. AVP:** Left panel shows an example of membrane potential responses of two pericytes during exposure to AVP (100 nM, similar to $n = 5$). Resting potentials prior to exposure were -61 mV and -62 mV. **C. ET1:** Left panel shows an example of membrane potential responses of two pericytes during exposure to Endothelin 1 (ET1, 1 nM, similar to $n = 5$). Resting potentials prior to exposure were -46 mV and -45 mV. For all constrictors, temporally similar variations of paired pericytes persisted throughout the recordings. Right panels show dashed lines of identity with individual data points of the adjacent records superimposed upon them.

doi:10.1371/journal.pone.0154948.g002

Table 1. Summary of linear regressions fit to dual pericyte membrane potential records during vasoconstrictor application.

	Configuration	Data points per record ^a	R value for linear regression ^b	n ^c	
AngII (10 nM)	Intact DVR	3750 ± 631	0.92 ± 0.06	5	NS ^d
AVP (100 nM)	Intact DVR	2538 ± 498	0.94 ± 0.04	5	NS ^d
ET1 (1 nM)	Intact DVR	2234 ± 526	0.94 ± 0.01	5	NS ^d
AngII (10 nM, P-P)	Isolated pericyte	3007 ± 624	0.91 ± 0.04	8	
AngII (10 nM, PxP)	Isolated pericyte	2800 ± 314	0.35 ± 0.05	8	P < 0.01 vs P-P

a, the mean ± SE of data points recorded for each vasoconstrictor

b, the mean ± SE of the “R” correlation coefficients of the linear regressions

c, n = number of recorded pericyte pairs = number of vessels = number of rats

d, NS; R values not significantly different from other vasoconstrictors by ANOVA.

doi:10.1371/journal.pone.0154948.t001

separation was imposed (**Fig 3C and 3D**, abbreviated PxP). Dual recordings during AngII (10 nM) stimulation derived from pericytes “in contact” (**Fig 4A, P-P**) yielded coordinated depolarizations like those in **Fig 2A**. In contrast, when cell-to-cell contact was disrupted (**Fig 4B, PxP**), pericyte depolarizations occurred but were not synchronized. Comparison of the mean ± SEM of correlation coefficients for n = 8 experiments in each configuration is shown in **Fig 4C** and summarized along with results from **Fig 2** in **Table 1**. Pericytes can share membrane potential and synchronize their responses in the absence of an endothelial layer.

Dual pericyte, endothelial recordings

We have previously shown that AngII stimulation depolarizes both the pericyte and endothelial layers of the DVR wall [17, 18]. To specifically test the separate ability of pericytes and endothelia to respond to AngII, we performed simultaneous dual-cell recording with configurations illustrated in **Fig 5**. Pericytes were either partially sheared from the vessel wall (**Fig 5A**, abbreviated P-E), so that the patched pericytes and endothelia remained physically associated, or pericytes were completely removed and deposited onto a coverslip adjacent to the denuded endothelium (**Fig 5B**, abbreviated PxE). In one series we used voltage clamp protocols to impose square wave membrane potential depolarizations on a pericyte while recording

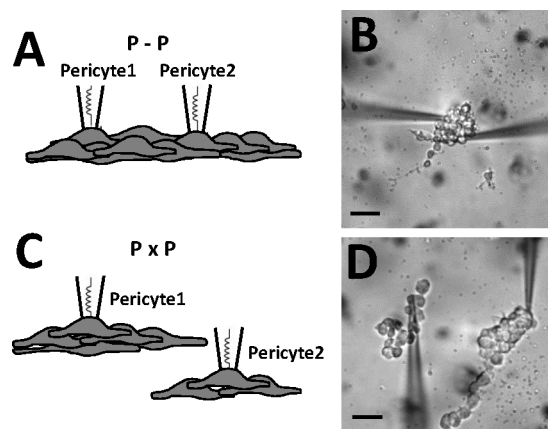


Fig 3. Simultaneous membrane potential recording from isolated pericytes; pericytes in contact. Schematic drawings and photomicrographs of dual recording from isolated pericytes in contact (**A, B**, designated P-P) on a coverslip or isolated without contact (**C, D**, designated PxP). The black bars = 10 microns.

doi:10.1371/journal.pone.0154948.g003

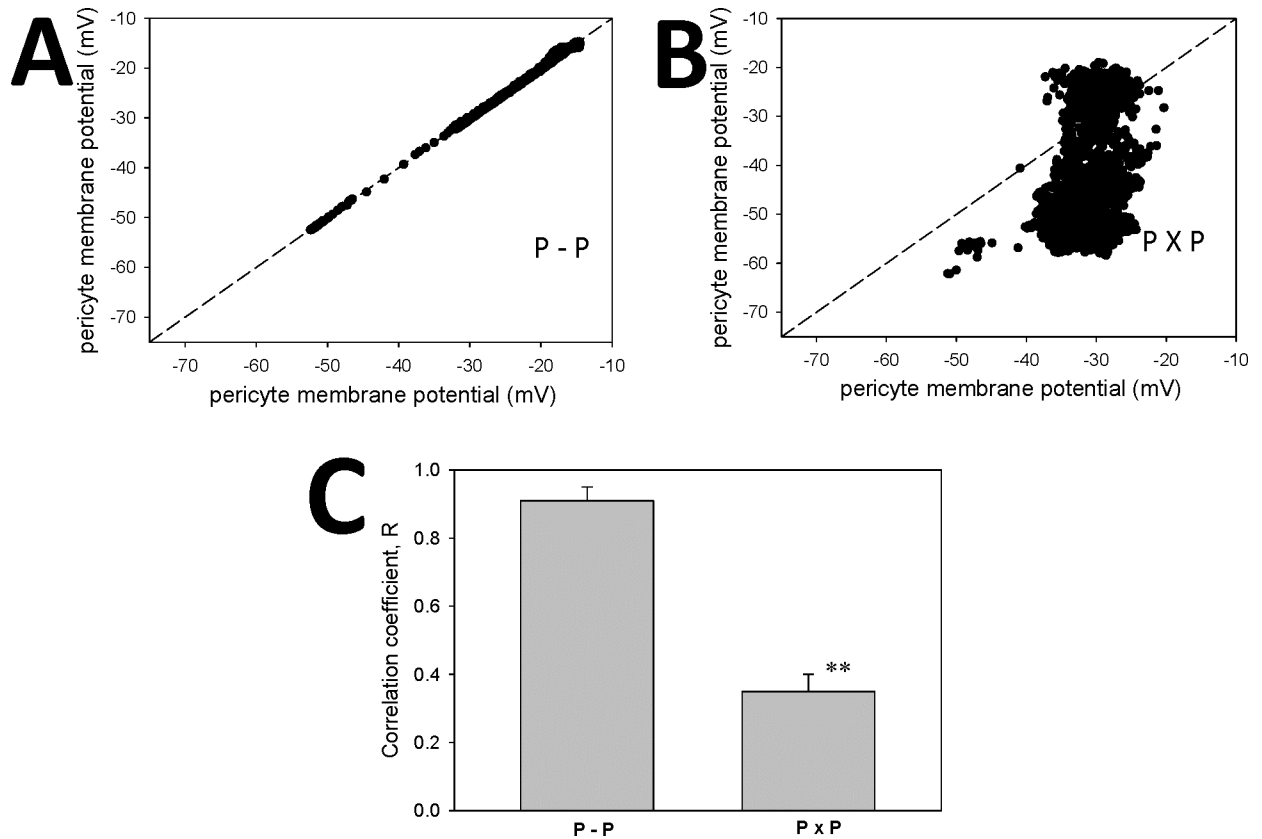


Fig 4. A. Single examples of AngII (10 nM) stimulated membrane potentials of paired pericytes isolated from endothelium, either in contact (A, P-P) or without contact (B, P x P). In each example the individual data points are superimposed upon the dashed line of identity. C. Summary of mean \pm SEM of correlation coefficients for P-P and P x P configurations (n = 8 each; **, P < 0.01). Other summaries are provided in [Table 1](#).

doi:10.1371/journal.pone.0154948.g004

transmission to a distant endothelial cell. We then introduced gap junction blockade heptanol, (2 mM) or 18B-glycyrrhetic acid (18BGR, 20 microM) to interfere with cell-to-cell transmission. As illustrated in the example [Fig 6A and 6B](#), the square-wave command potential imposed on the pericyte was reproduced distantly in the endothelium. The communicated endothelial response was reversibly attenuated, but not eliminated, by gap junction blockade with heptanol ([Fig 6B](#)). Averaged results for heptanol are shown in [Fig 6C](#) (n = 6). Averaged results for 18BGR are shown in [Fig 6D](#) (n = 8).

In another series, we measured simultaneous membrane potential responses of pericytes and endothelia to AngII exposure when the cells were either in communication on an intact vessel as in [Fig 5A](#) (P-E), or isolated from one another as in [Fig 5B](#) (PxE). As previously reported [18], when in contact, resting membrane potentials were very similar, with endothelia slightly hyperpolarized relative to pericytes ([Fig 7A and 7B](#)). When pericytes were fully isolated from the endothelium, resting potentials remained similar in magnitude ([Fig 7C](#)) but were not correlated ([Fig 7D](#)) and the relative endothelial hyperpolarization no longer persisted (compare [Fig 7A and 7C](#)). Finally, when AngII response was measured in partially denuded vessels as in [Fig 5A](#) (P-E), pericyte and endothelial membrane potentials remained highly coordinated ([Fig 8A and 8B](#)) [18]. In contrast, total isolation of pericytes from endothelia as in [Fig 5B](#) (PxE) completely eliminated AngII induced endothelial depolarizations ([Fig 8C and 8D](#)). As summarized in [Fig 9](#) these results were highly consistent.

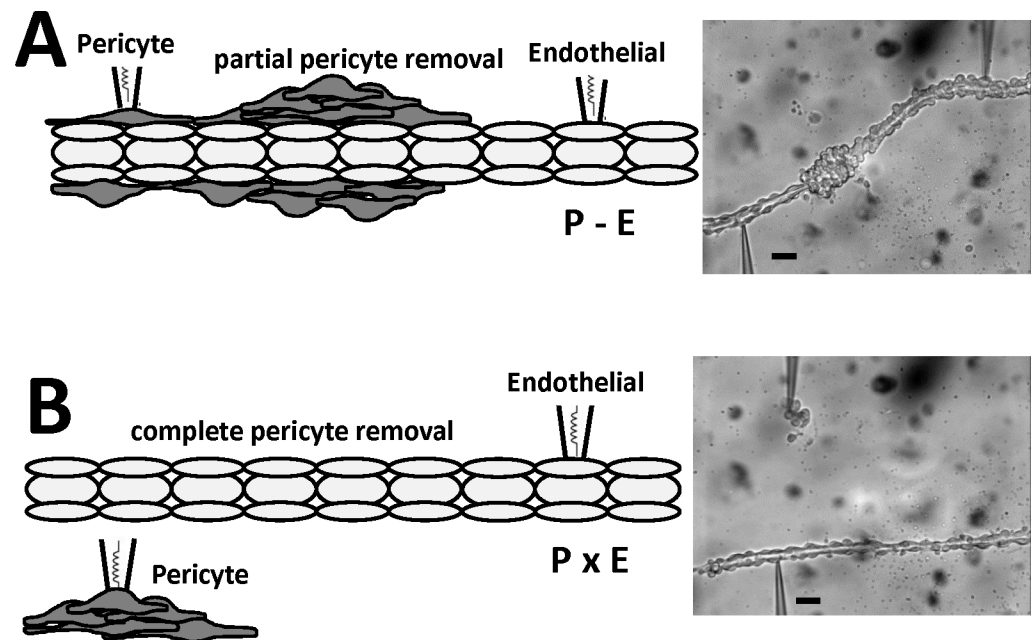


Fig 5. Configurations for simultaneous recording from DVR pericytes and endothelia. **A.** Left and right panels show schematic depiction and photomicrograph of a partially denuded DVR with simultaneous dual-cell patch clamp of a pericyte and an endothelial cell that retain contact (abbreviated P-E). **B.** Left and right panels show a schematic depiction and photomicrograph of a DVR, fully denuded of pericytes, with simultaneous dual-cell patch clamp of each cell type when they have no contact (abbreviated P x E). These configurations were used to test the importance of cell contact for AngII dependent membrane potential responses. The black bars = 10 microns.

doi:10.1371/journal.pone.0154948.g005

Discussion

Syncytial communication of the vasculature is thought to be most prominent in microvessels [9, 19, 20]. The ability of the vessel wall to accommodate mural conduction of depolarizing and hyperpolarizing signals probably serves to extend their spatial influence to upstream locations [19, 21]. In the renal medulla, where access, *in vivo* is impossible, this is an unproven but inviting prospect. It is widely believed that countercurrent trapping leads to progressive hypoxia with medullary depth, predisposing to tissue injury [22, 23]. Hypothetically, the ability of the DVR wall to carry vasodilatory hyperpolarization toward their parent juxtamedullary efferent arterioles could be important to matching metabolic demands and blood supply. By that scheme, hyperpolarization from adenosine, NO, CO, EETs or other diffusible activators released from interbundle epithelia might generate feedback responses to rescue their oxygenation [24–26]. DVR also generate their own intrinsic signals in the form of endothelium dependent relaxing and hyperpolarizing factors. Intrinsic NO release has major influence on the tone of isolated DVR [19]. Moreover, strong inward rectifier K^+ channels and K_{ATP} channels are expressed to favor their combined syncytial hyperpolarization by extracellular K^+ ion or other EDHFs [27, 28]. Finally, not to be discounted in this scheme, mechanical forces such as endothelial shear or tissue compression via ureteral peristalsis probably stimulate electrical responses within the DVR wall. Shear dependent NO release has been demonstrated [29] and mechanical perturbation of the abluminal surface induces brisk, reversible depolarizations and calcium elevations that spread along the vessel axis by mural conduction. The latter were found to be sensitive to either gap junction or L-type VGCC blockade [30].

Similar to juxtamedullary efferent arteriolar smooth muscle [31], DVR express VGCC and electrophysiological recordings have shown nifedipine-sensitive L-type Ca^{2+} / Ba^{2+} currents in

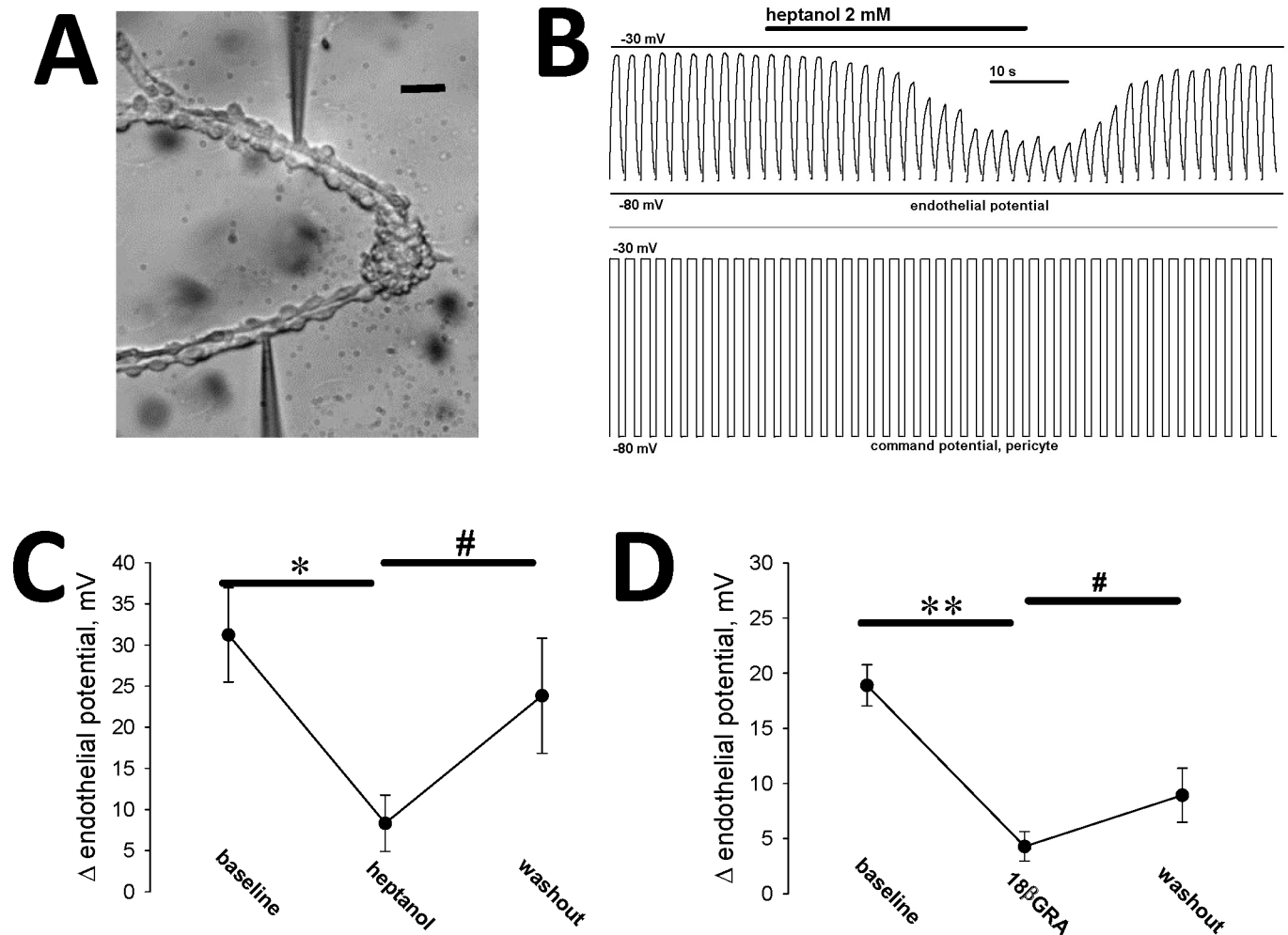


Fig 6. Dual recording from pericyte and endothelium during AngII exposure and gap junction blockade. **A.** Photomicrograph of the dual pericyte, endothelial preparation that yielded the recording in panel B. The black bar = 10 microns. **B.** Electrophysiological record; square wave depolarizations from -80 to -30 mV were imposed at regular intervals on a voltage clamped pericyte. The endothelial response during pericyte depolarization (top) and the pericyte command potential (bottom) are shown before, during and after application of heptanol (2 mM). **C.** Summary of experiments similar to that shown in panel B. The average membrane potential deviation of the endothelium is shown before, during and after washout of heptanol, which reversibly attenuated conduction (mean ± SEM, n = 6). Repeated measures ANOVA, DF = 17, F = 19.5, P < 0.001. By Holm-Sidak multiple comparison; * P < 0.05 baseline vs heptanol, # P < 0.05, heptanol vs washout. **D.** Summary of experiments similar to that shown in panel B, but with 18βGRA (20 microM) as the gap junction blocker (mean ± SEM, n = 8). Repeated measures ANOVA, DF = 23, F = 38.6, P < 0.001. By Holm-Sidak multiple comparison; ** P < 0.01 baseline vs 18βGRA, # P < 0.05 18βGRA vs washout.

doi:10.1371/journal.pone.0154948.g006

DVR pericytes [4]. Stimulation by vasoconstrictors induces depolarization that opens VGCC following activation of CaCC. Concomitant suppression of K⁺ conductance augments durability of the attendant rise in membrane potential [6, 7]. As such, control of membrane potential and conduction of it between cells regulates DVR vessel tone. Given that DVR supply the medulla at various depths, depending on their location within vascular bundles, it is reasonable to surmise that similar events may play a pivotal role to regulate blood flow distribution within the medulla. This notion is favored by studies of changes in medullary blood following global VGCC blockade [32–34].

The goal of the present study was to define the routes by which membrane potential can be conducted within the DVR wall. Depolarizing responses might spread via gap junctions between pericytes. Alternately, the conduction might involve only myo-endothelial conduction

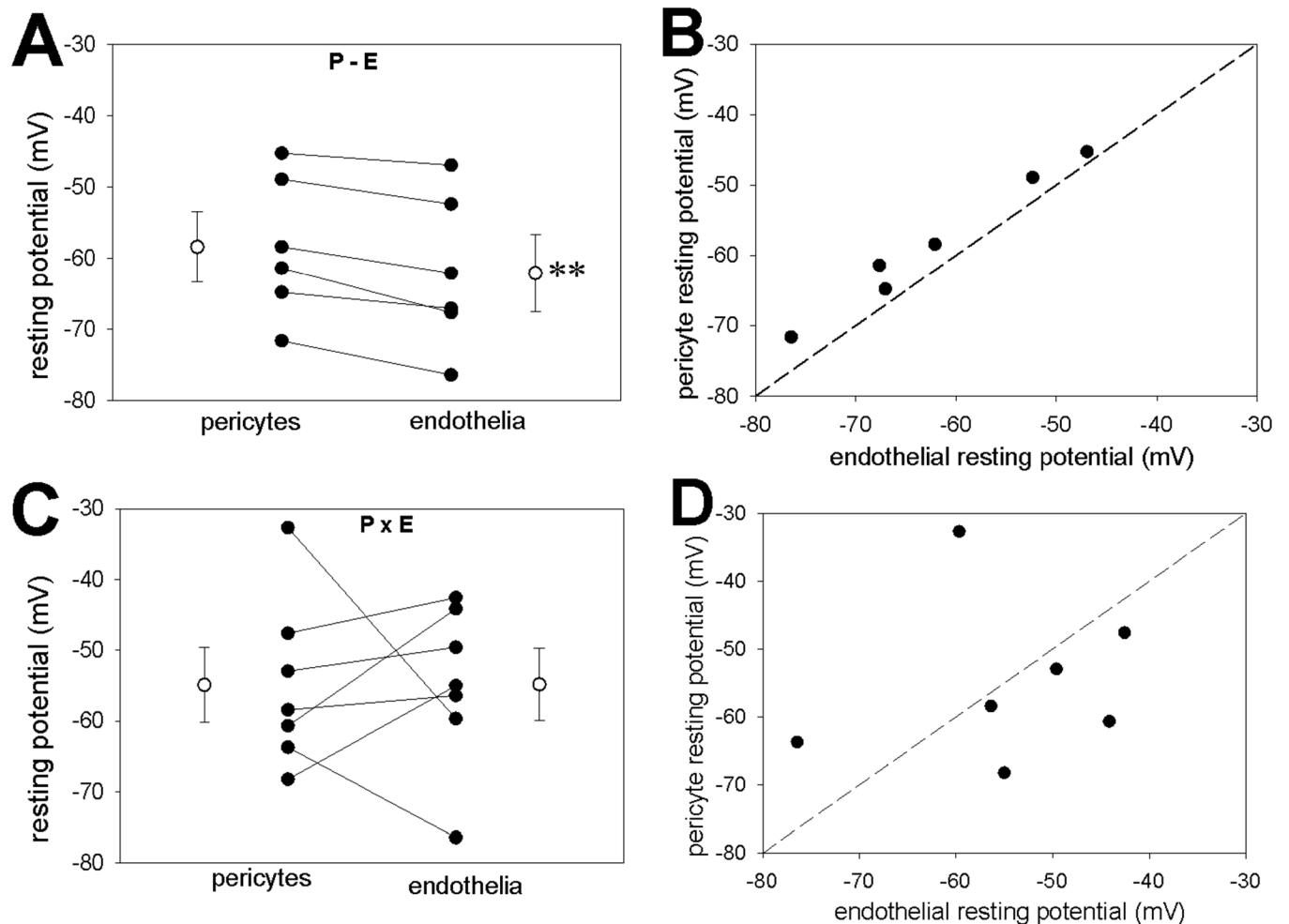


Fig 7. Dual recording from pericytes and endothelia during AngII exposure, cells associated or spatially separated. **A.** Resting potential of pericytes and endothelia that are associated on the DVR wall (as in Fig 5A). Endothelial cells were significantly hyperpolarized relative to the pericytes (paired t-test, $n = 6$, $** P < 0.01$). **B.** Simultaneous endothelial and pericyte resting membrane potentials from panel A superimposed on the line of identity. By linear regression, values were highly correlated (DF = 5, $F = 221$, $R = 0.99$, $P < 0.001$). **C.** Resting potential of pericytes and endothelia dissociated from one another (as in Fig 5B). Resting potentials were not significantly different ($n = 7$). **D.** Simultaneous endothelial and pericyte resting membrane potentials from panel C superimposed on the line of identity. A significant correlation was not observed (DF = 6, $F = 0.13$, $R = 0.16$, $P = 0.73$).

doi:10.1371/journal.pone.0154948.g007

such that membrane potential changes originating from a pericyte must conduct in sequence through the endothelium and then to nearby pericytes. Finally, the origins of endothelial voltage responses to agonists are uncertain. Do AngII responses of endothelia depend upon endothelial receptors, or are the responses conducted from temporal changes that occur within adjacent pericytes? Since gap junction blockers have nonspecific actions and genetic manipulation of connexins might alter compositions of connexon proteins, we utilized physical disruption of cell-to-cell communication to explore these questions. Our results show that pericytes on the wall of an isolated DVR segment have nearly identical membrane potentials (Fig 1). Within the limits of spatial separation afforded by DVR isolation (i.e., 300 to 1000 microns), the syncytial sharing of voltage between pericytes seems robust.

Connexons form gap junction intercellular channels with variable conductance, open probabilities and sub conductance states [9, 35]. As such, they might be regulated by differences in membrane potential between the cells they couple, or by covalent modifications of their

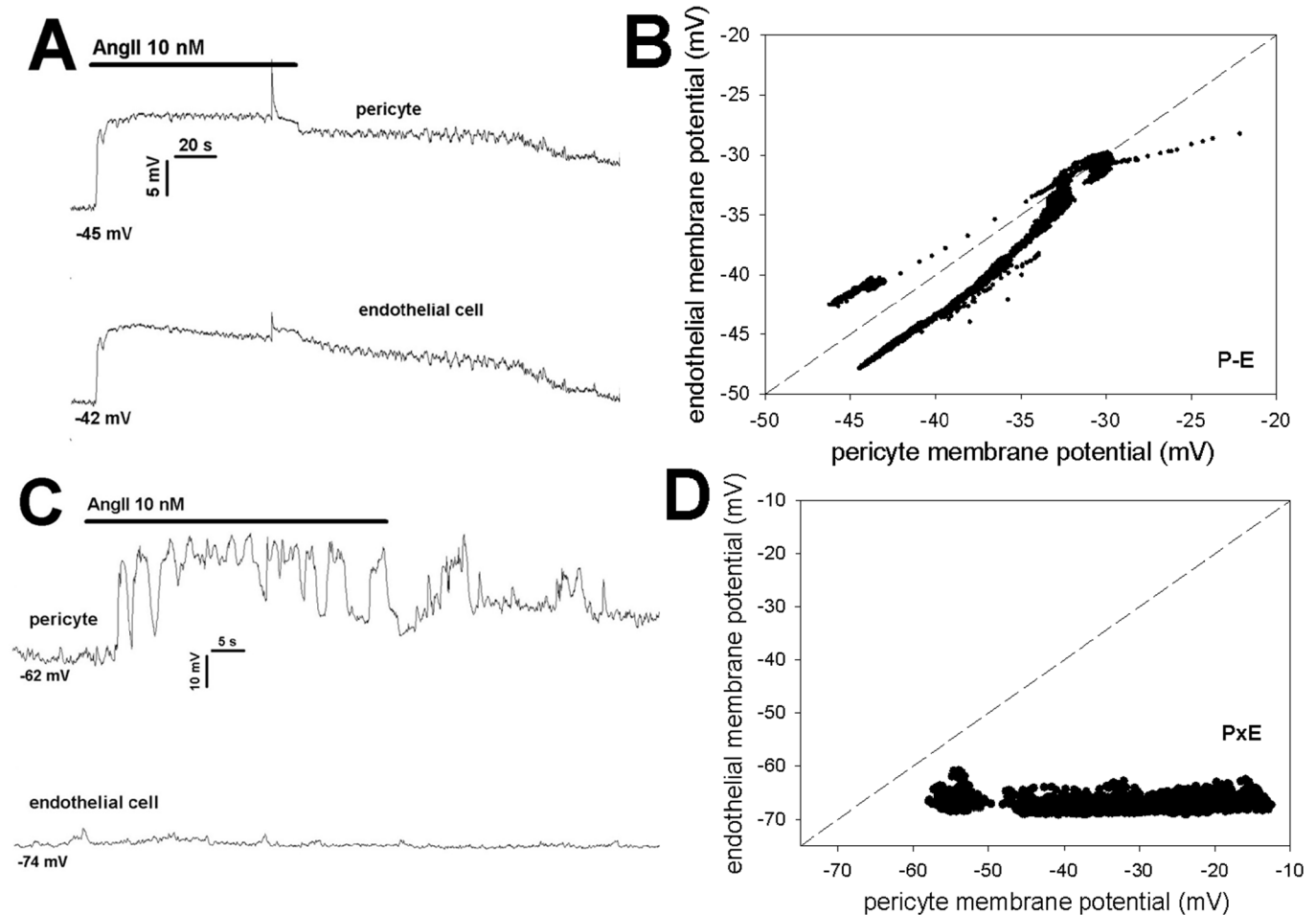


Fig 8. Simultaneous pericyte, endothelial membrane potential responses to AngII with and without cell contact. **A.** Example of AngII induced membrane potential responses of a pericyte and an endothelial cell physically associated with one another along the DVR wall (as in Fig 5A). Similar time dependent variations persisted throughout the record. Resting potentials prior to AngII were -45 mV and -42 mV. **B.** Individual data points of the record in panel A are shown superimposed upon the line of identity. Throughout most of the record, the endothelium remained hyperpolarized relative to the pericyte. **C.** Example of AngII induced membrane potential responses of a pericyte and an endothelial cell when cells were dissociated (as in Fig 5B). Membrane potential variations were observed in the pericyte but not in the endothelial cell. Resting potentials prior to AngII were -62 mV and -74 mV. **D.** Individual data points of panel A are shown superimposed upon the line of identity. Pericyte response occurred but a concomitant endothelial response was absent.

doi:10.1371/journal.pone.0154948.g008

subunits downstream of signaling events [36]. For example phosphorylation of connexins 37, 40 and 43 affect cell-to-cell communications in varying ways [36–38]. We measured the equivalence of pericyte membrane potentials after vasoactive stimulation by AngII, AVP or ET1, each of which are known to constrict DVR. A persistent, robust coordination between cells was always retained (Fig 2). Moreover, even after pericytes were isolated from the endothelium, they coordinated responses between themselves, implying that gap junctions between pericytes are sufficient to conduct electrical activity (Fig 4).

We previously demonstrated that endothelial membrane potential closely tracks that of nearby pericytes, while remaining a few millivolts hyperpolarized to them. Likely, this relationship provides a braking effect so that pericyte depolarization is blunted and VGCC mediated Ca^{2+} entry and consequent DVR constriction is self-limited. In contrast to the close parallel voltage changes of adjacent pericytes and endothelium, parallel changes of cytoplasmic Ca^{2+} (Ca_{CYT}) does not occur. When AngII induces oscillatory or persistent increases in pericyte

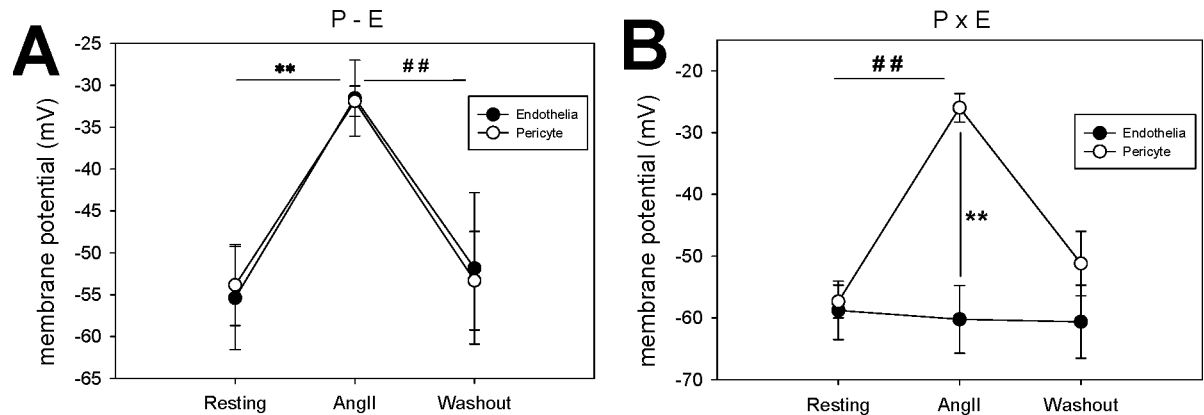


Fig 9. Summary of simultaneous pericyte and endothelial membrane potential responses to AngII with and without cell contact. **A.** Summary of average membrane potential before (resting), during peak depolarization (AngII), and after washout ($n = 6$, P-E configuration, as in Fig 5A). The depolarizations (mean \pm SEM) were significant (repeated measures ANOVA, $DF = 17$, $F = 12.9$, $P < 0.01$). By Holm-Sidak multiple comparison; **, $P < 0.01$ resting vs AngII, ##, $P < 0.01$ AngII vs washout. Pericyte and endothelial depolarizations were nearly identical (no significant differences between cell types). **B.** Summary of average membrane potentials before, during AngII, and after washout ($n = 6$, Px E configuration as in Fig 5A). The pericyte depolarizations (mean \pm SEM) were significant (repeated measures ANOVA, $DF = 17$, $F = 53.5$, $P < 0.01$). By Holm-Sidak multiple comparison; ##, $P < 0.01$ resting vs AngII or AngII vs washout. In contrast to the P-E configuration, in the absence of pericyte contact, AngII did not alter endothelial membrane potential; (group t-test, ** $P < 0.01$ endothelia vs pericytes during AngII exposure).

doi:10.1371/journal.pone.0154948.g009

Ca_{CYT} , endothelial Ca_{CYT} is suppressed [39, 40]. Similarly, mechanical stimulation of the pericyte surface depolarizes them, elevates pericyte Ca_{CYT} and generates conducted Ca_{CYT} elevations along the vessel axis. During that response, concomitant endothelial Ca_{CYT} changes are small or absent [30]. Thus, any monovalent ion movements responsible for coordination of membrane potential fluctuations may not be accompanied by cell-to-cell divalent ion fluxes. If divalent flux across gap junctions does occur the effects on cytoplasmic concentrations may be rapidly blunted cytoplasmic buffering mechanisms [41].

The existence of AngII receptors on DVR endothelia has been uncertain [39]. It is possible that endothelial responses are mediated by the coordination of membrane potential changes alone (Figs 5–8), or by diffusion of secondary signaling molecules across myo-endothelial junctions. We separated the cells of native isolated DVR to test the possibilities (Fig 5). Square wave pericyte depolarizations imposed by voltage clamp were conducted to endothelia and sensitive to chemical gap junction blockade (Fig 6). Mechanical removal of pericytes from the DVR wall eliminated close correlation between pericyte and endothelial resting potentials (Fig 7). Moreover, it fully eliminated the ability of AngII to depolarize DVR endothelia (Figs 8 and 9). These data support the interpretation that expression of AngII receptors on DVR endothelia might account for DVR endothelial electrical responses. Rather, conductance via myo-endothelial junctions may yield such changes. AngII lowers Ca_{CYT} in DVR endothelia [39, 40]. This too might result from depolarization. If endothelial VGCC are absent and extracellular calcium is conducted into the endothelial cytoplasm through voltage independent cation channels, e.g., TRP isoforms [42], the reduction in electrochemical gradient that accompanies depolarization might be sufficient to diminish the Ca^{2+} influx rate and account for Ca_{CYT} suppression. The precise relationship between endothelial Ca_{CYT} and membrane potential remains an area of investigation [43].

Connexin (Cx) isoforms associate in homologous and heterologous combinations to form gap junction proteins that dock to form channel-like conduits between cells [44]. Immunostaining of the DVR wall identified expression of Cx37, Cx40 and Cx43 which are commonly found in the vasculature [45]. Those isoforms and Cx45 [46] are expressed in arterioles in the

renal cortex where vascular gap communication may coordinate oscillatory pressure fluctuations of adjacent nephrons [47, 48], modify transmission of systemic pressure to glomeruli and play roles in renin release [49–51]. Such behavior is not unique to the kidney. Recognition of the existence of vasomotion and calcium waves in the microvasculature of various organ beds has been longstanding. It is broadly accepted that oscillatory variations of membrane potential and Ca_{CYT} , manifested as vasomotion, is coordinated via smooth muscle and endothelial gap junctions [52]. Disease states such as atherosclerosis and diabetes lead to changes in vasoactivity, but the physiological role(s) and consequences of modifying normal activity continues to be unclear. Studies in the renal cortex where surface vessels are accessible have yielded some intriguing results. The range over which such coupling occurs had been thought to be small. Simultaneous measurements of nephron activity using micropuncture methods are technically limited, but more recent observations over broader areas of the cortex using laser-speckle imaging has revealed extended synchronization. This implies possible coordination via interlobular arterioles and their attendant regions of perfusion [53, 54]. Study of the implications of this seminal finding for salt and water homeostasis, glomerular hypertension, and kidney disease is in infant stages and will be of much interest. Diminished synchronization between nephrons in hypertensive states has already been shown [55]. With regard to the renal outer medulla, where vascular bundles are inaccessible in vivo, studies of coordination of tissue perfusion remain absent.

There are limitations to interpretation of these studies. Outer medullary DVR are inaccessible in vivo in a region of the kidney where oxygen tensions are low and osmolality higher than systemic plasma. The precise concentrations of electrolytes and urea cannot be known with certainty. Our experimental conditions cannot replicate that environmental milieu its osmolality or oxygen tensions. Our buffers do not contain the repertoire of paracrine agents that must certainly exist in renal outer medullary vascular bundles, in vivo. As such, extrapolation of these results to predict renal medullary physiology must be done with uncertainty and caution.

Acknowledgments

These studies have been supported by NIH grants R01DK042495 and R01DK067621.

Author Contributions

Conceived and designed the experiments: ZZ TLP. Performed the experiments: ZZ KP. Analyzed the data: ZZ KP TLP. Wrote the paper: TLP.

References

1. Pallone TL, Turner MR, Edwards A, Jamison RL. Countercurrent exchange in the renal medulla. *Am J Physiol Regul Integr Comp Physiol*. 2003; 284(5):R1153–R1175.
2. Pannabecker TL, Dantzier WH. Three-dimensional architecture of inner medullary vasa recta. *Am J Physiol Renal Physiol*. 2006; 290(6):F1355–66. PMID: [16380456](#)
3. Schwartz MM, Karnovsky MJ, Vehkatchalam MA. Ultrastructural differences between rat inner medullary descending and ascending vasa recta. *Laboratory investigation; a journal of technical methods and pathology*. 1976; 35(2):161–70. PMID: [957604](#)
4. Zhang Z, Lin H, Cao C, Khurana S, Pallone TL. Voltage-gated divalent currents in descending vasa recta pericytes. *Am J Physiol Renal Physiol*. 2010; 299(4):F862–71. doi: [10.1152/ajprenal.00321.2010](#) PMID: [20630935](#)
5. Zhang Z, Rhinehart K, Pallone TL. Membrane potential controls calcium entry into descending vasa recta pericytes. *Am J Physiol Regul Integr Comp Physiol*. 2002; 283(4):R949–R957.
6. Pallone TL, Cao C, Zhang Z. Inhibition of K^+ conductance in descending vasa recta pericytes by ANG II. *Am J Physiol Renal Physiol*. 2004; 287(6):F1213–F22.

7. Pallone TL, Huang JM. Control of descending vasa recta pericyte membrane potential by angiotensin II. *AmJPhysiol Renal Physiol*. 2002; 282(6):F1064–F74.
8. de Wit C, Griffith TM. Connexins and gap junctions in the EDHF phenomenon and conducted vasomotor responses. *Pflugers Arch*. 2010; 459(6):897–914. doi: [10.1007/s00424-010-0830-4](https://doi.org/10.1007/s00424-010-0830-4) PMID: [20379740](https://pubmed.ncbi.nlm.nih.gov/20379740/)
9. Figueroa XF, Isakson BE, Duling BR. Connexins: gaps in our knowledge of vascular function. *Physiology (Bethesda)*. 2004; 19:277–84.
10. Verselis VK, Srinivas M. Connexin channel modulators and their mechanisms of action. *Neuropharmacology*. 2013; 75:517–24. doi: [10.1016/j.neuropharm.2013.03.020](https://doi.org/10.1016/j.neuropharm.2013.03.020) PMID: [23597508](https://pubmed.ncbi.nlm.nih.gov/23597508/)
11. Pallone TL, Work J, Myers RL, Jamison RL. Transport of sodium and urea in outer medullary descending vasa recta. *JClinInvest*. 1994; 93(1):212–22.
12. Zhang Z, Rhinehart K, Kwon W, Weinman E, Pallone TL. ANG II signaling in vasa recta pericytes by PKC and reactive oxygen species. *AmJPhysiol Heart CircPhysiol*. 2004; 287(2):H773–H81.
13. Zhang Z, Lin H, Cao C, Payne K, Pallone TL. Descending vasa recta endothelial cells and pericytes form mural syncytia. *Am J Physiol Renal Physiol*. 2013.
14. Turner MR, Pallone TL. Vasopressin constricts outer medullary descending vasa recta isolated from rat kidneys. *AmJPhysiol*. 1997; 272(1 Pt 2):F147–F51.
15. Silldorff EP, Yang S, Pallone TL. Prostaglandin E2 abrogates endothelin-induced vasoconstriction in renal outer medullary descending vasa recta of the rat. *JClinInvest*. 1995; 95(6):2734–40.
16. Pallone TL. Vasoconstriction of outer medullary vasa recta by angiotensin II is modulated by prostaglandin E2. *AmJPhysiol*. 1994; 266(6 Pt 2):F850–F7.
17. Rhinehart K, Zhang Z, Pallone TL. Ca(2+) signaling and membrane potential in descending vasa recta pericytes and endothelia. *AmJPhysiol Renal Physiol*. 2002; 283(4):F852–F60.
18. Zhang Z, Payne K, Pallone TL. Syncytial communication in descending vasa recta includes myoendothelial coupling. *Am J Physiol Renal Physiol*. 2014; 307(1):F41–52. doi: [10.1152/ajprenal.00178.2014](https://doi.org/10.1152/ajprenal.00178.2014) PMID: [24785189](https://pubmed.ncbi.nlm.nih.gov/24785189/)
19. Cao C, Edwards A, Sendeski M, Lee-Kwon W, Cui L, Cai CY, et al. Intrinsic nitric oxide and superoxide production regulates descending vasa recta contraction. *Am J Physiol Renal Physiol*. 2010; 299(5): F1056–64. doi: [10.1152/ajprenal.00070.2010](https://doi.org/10.1152/ajprenal.00070.2010) PMID: [20702600](https://pubmed.ncbi.nlm.nih.gov/20702600/)
20. De Wit C. Connexins pave the way for vascular communication. *News Physiol Sci*. 2004; 19:148–53. PMID: [15143212](https://pubmed.ncbi.nlm.nih.gov/15143212/)
21. Garland CJ, Hiley CR, Dora KA. EDHF: spreading the influence of the endothelium. *Br J Pharmacol*. 2011; 164(3):839–52. doi: [10.1111/j.1476-5381.2010.01148.x](https://doi.org/10.1111/j.1476-5381.2010.01148.x) PMID: [21133895](https://pubmed.ncbi.nlm.nih.gov/21133895/)
22. Heyman SN, Rosenberger C, Rosen S. Regional alterations in renal haemodynamics and oxygenation: a role in contrast medium-induced nephropathy. *Nephrol Dial Transplant*. 2005; 20 Suppl 1:i6–11. PMID: [15705946](https://pubmed.ncbi.nlm.nih.gov/15705946/)
23. Evans RG, Eppel GA, Anderson WP, Denton KM. Mechanisms underlying the differential control of blood flow in the renal medulla and cortex. *J Hypertens*. 2004; 22(8):1439–51. PMID: [15257161](https://pubmed.ncbi.nlm.nih.gov/15257161/)
24. O'Connor PM, Cowley AW Jr. Medullary thick ascending limb buffer vasoconstriction of renal outer-medullary vasa recta in salt-resistant but not salt-sensitive rats. *Hypertension*. 2012; 60(4):965–72. doi: [10.1161/HYPERTENSIONAHA.112.195214](https://doi.org/10.1161/HYPERTENSIONAHA.112.195214) PMID: [22926950](https://pubmed.ncbi.nlm.nih.gov/22926950/)
25. Pallone TL, Zhang Z, Rhinehart K. Physiology of the renal medullary microcirculation. *AmJPhysiol Renal Physiol*. 2003; 284(2):F253–F66.
26. Dickhout JG, Mori T, Cowley AW Jr. Tubulovascular nitric oxide crosstalk: buffering of angiotensin II-induced medullary vasoconstriction. *Circ Res*. 2002; 91(6):487–93. PMID: [12242266](https://pubmed.ncbi.nlm.nih.gov/12242266/)
27. Cao C, Goo JH, Lee-Kwon W, Pallone TL. Vasa recta pericytes express a strong inward rectifier K+ conductance. *AmJPhysiol RegulIntegrComp Physiol*. 2006; 290(6):R1601–R7.
28. Cao C, Lee-Kwon W, Payne K, Edwards A, Pallone TL. Descending vasa recta endothelia express inward rectifier potassium channels. *AmJPhysiol Renal Physiol*. 2007; 293(4):F1248–F55.
29. Zhang Z, Pallone TL. Response of descending vasa recta to luminal pressure. *AmJPhysiol Renal Physiol*. 2004; 287(3):F535–F42.
30. Zhang Z, Payne K, Cao C, Pallone TL. Mural propagation of descending vasa recta responses to mechanical stimulation. *Am J Physiol Renal Physiol*. 2013; 305(3):F286–94. doi: [10.1152/ajprenal.00220.2013](https://doi.org/10.1152/ajprenal.00220.2013) PMID: [23698119](https://pubmed.ncbi.nlm.nih.gov/23698119/)
31. Hansen PB. Functional and pharmacological consequences of the distribution of voltage-gated calcium channels in the renal blood vessels. *Acta Physiol (Oxf)*. 2013; 207(4):690–9.
32. Hansell P, Nygren A, Ueda J. Influence of verapamil on regional renal blood flow: a study using multichannel laser-Doppler flowmetry. *Acta physiologica Scandinavica*. 1990; 139(1):15–20. PMID: [2192538](https://pubmed.ncbi.nlm.nih.gov/2192538/)

33. Lu S, Roman RJ, Mattson DL, Cowley AW, Jr. Renal medullary interstitial infusion of diltiazem alters sodium and water excretion in rats. *The American journal of physiology*. 1992; 263(5 Pt 2):R1064–70. PMID: [1443224](#)
34. Yagil Y, Miyamoto M, Frasier L, Oizumi K, Koike H. Effects of CS-905, a novel dihydropyridine calcium channel blocker, on arterial pressure, renal excretory function, and inner medullary blood flow in the rat. *American journal of hypertension*. 1994; 7(7 Pt 1):637–46. PMID: [7946166](#)
35. Sorensen CM, Holstein-Rathlou NH. Cell-cell communication in the kidney microcirculation. *Microcirculation (New York, NY: 1994)*. 2012; 19(5):451–60.
36. de Wit C, Wolffe SE, Hopfl B. Connexin-dependent communication within the vascular wall: contribution to the control of arteriolar diameter. *Adv Cardiol*. 2006; 42:268–83. PMID: [16646597](#)
37. Hoffmann A, Gloe T, Pohl U, Zahler S. Nitric oxide enhances de novo formation of endothelial gap junctions. *Cardiovasc Res*. 2003; 60(2):421–30. PMID: [14613872](#)
38. Kameritsch P, Hoffmann A, Pohl U. Opposing effects of nitric oxide on different connexins expressed in the vascular system. *Cell communication & adhesion*. 2003; 10(4–6):305–9.
39. Pallone TL, Silldorff EP, Zhang Z. Inhibition of calcium signaling in descending vasa recta endothelia by ANG II. *AmJPhysiol Heart CircPhysiol*. 2000; 278(4):H1248–H55.
40. Zhang Q, Cao C, Zhang Z, Wier WG, Edwards A, Pallone TL. Membrane current oscillations in descending vasa recta pericytes. *Am J Physiol Renal Physiol*. 2008; 294(3):F656–66. doi: [10.1152/ajprenal.00493.2007](#) PMID: [18184740](#)
41. Parekh AB. Ca²⁺ microdomains near plasma membrane Ca²⁺ channels: impact on cell function. *J Physiol*. 2008; 586(Pt 13):3043–54.
42. Nilius B, Droogmans G, Wondergem R. Transient receptor potential channels in endothelium: solving the calcium entry puzzle? *Endothelium*. 2003; 10(1):5–15. PMID: [12699072](#)
43. Dora KA, Garland CJ. Linking hyperpolarization to endothelial cell calcium events in arterioles. *Microcirculation (New York, NY: 1994)*. 2013; 20(3):248–56.
44. Evans WH, Martin PE. Gap junctions: structure and function (Review). *Mol Membr Biol*. 2002; 19(2):121–36. PMID: [12126230](#)
45. Zhang Q, Cao C, Mangano M, Zhang Z, Silldorff EP, Lee-Kwon W, et al. Descending vasa recta endothelium is an electrical syncytium. *AmJPhysiol Regul Integr Comp Physiol*. 2006; 291(6):R1688–R99.
46. Hanner F, Sorensen CM, Holstein-Rathlou NH, Peti-Peterdi J. Connexins and the kidney. *Am J Physiol Regul Integr Comp Physiol*. 2010; 298(5):R1143–55. doi: [10.1152/ajpregu.00808.2009](#) PMID: [20164205](#)
47. Holstein-Rathlou NH. Synchronization of proximal intratubular pressure oscillations: evidence for interaction between nephrons. *Pflugers Arch*. 1987; 408(5):438–43. PMID: [3601634](#)
48. Holstein-Rathlou NH, Marsh DJ. Oscillations of tubular pressure, flow, and distal chloride concentration in rats. *The American journal of physiology*. 1989; 256(6 Pt 2):F1007–14. PMID: [2735418](#)
49. Wagner C, Kurtz A. Distribution and functional relevance of connexins in renin-producing cells. *Pflugers Arch*. 2013; 465(1):71–7. doi: [10.1007/s00424-012-1134-7](#) PMID: [22744230](#)
50. Hanner F, von Maltzahn J, Maxeiner S, Toma I, Sipos A, Kruger O, et al. Connexin45 is expressed in the juxtaglomerular apparatus and is involved in the regulation of renin secretion and blood pressure. *Am J Physiol Regul Integr Comp Physiol*. 2008; 295(2):R371–80. doi: [10.1152/ajpregu.00468.2007](#) PMID: [18579650](#)
51. Kurtz L, Gerl M, Kriz W, Wagner C, Kurtz A. Replacement of connexin 40 by connexin 45 causes ectopic localization of renin-producing cells in the kidney but maintains in vivo control of renin gene expression. *Am J Physiol Renal Physiol*. 2009; 297(2):F403–9. doi: [10.1152/ajprenal.00176.2009](#) PMID: [19474190](#)
52. Aalkjaer C, Boedtker D, Matchkov V. Vasomotion—what is currently thought? *Acta Physiol (Oxf)*. 2011; 202(3):253–69.
53. Holstein-Rathlou NH, Sosnovtseva OV, Pavlov AN, Cupples WA, Sorensen CM, Marsh DJ. Nephron blood flow dynamics measured by laser speckle contrast imaging. *Am J Physiol Renal Physiol*. 2011; 300(2):F319–29. doi: [10.1152/ajprenal.00417.2010](#) PMID: [21048025](#)
54. Mitrou N, Scully CG, Braam B, Chon KH, Cupples WA. Laser speckle contrast imaging reveals large-scale synchronization of cortical autoregulation dynamics influenced by nitric oxide. *Am J Physiol Renal Physiol*. 2015; 308(7):F661–70. doi: [10.1152/ajprenal.00022.2014](#) PMID: [25587114](#)
55. Yip KP, Holstein-Rathlou NH, Marsh DJ. Dynamics of TGF-initiated nephron-nephron interactions in normotensive rats and SHR. *The American journal of physiology*. 1992; 262(6 Pt 2):F980–8. PMID: [1621821](#)